



Beam shape coefficients calculation for an elliptical Gaussian beam with 1-dimensional quadrature and localized approximation methods

Wei Wang, Jianqi Shen*

University of Shanghai for Science and Technology, Shanghai 200093, China

ARTICLE INFO

Article history:

Received 4 January 2018

Revised 31 March 2018

Accepted 31 March 2018

Available online 7 April 2018

Keywords:

Quadrature method

Beam shape coefficient

Elliptical Gaussian beam

Light scattering

ABSTRACT

The use of a shaped beam for applications relying on light scattering depends much on the ability to evaluate the beam shape coefficients (BSC) effectively. Numerical techniques for evaluating the BSCs of a shaped beam, such as the quadrature, the localized approximation (LA), the integral localized approximation (ILA) methods, have been developed within the framework of generalized Lorenz-Mie theory (GLMT). The quadrature methods usually employ the 2-/3-dimensional integrations. In this work, the expressions of the BSCs for an elliptical Gaussian beam (EGB) are simplified into the 1-dimensional integral so as to speed up the numerical computation. Numerical results of BSCs are used to reconstruct the beam field and the fidelity of the reconstructed field to the given beam field is estimated. It is demonstrated that the proposed method is much faster than the 2-dimensional integrations and it can acquire more accurate results than the LA method. Limitations of the quadrature method and also the LA method in the numerical calculation are analyzed in detail.

© 2018 Elsevier Ltd. All rights reserved.

1. Introduction

Most laser diodes or solid-state lasers emit elliptical Gaussian beams. The use of EGBs is of growing interest in measurement techniques relying on light scattering such as optical sizing, particle image velocimetry, optical trapping, manipulation and etc [1–5], which depends much on the ability to evaluate the BSCs efficiently. Within the GLMT framework for describing the interaction between a shaped beam and a spherical particle, one must first have a physical description of the beam in terms of radial electrical and magnetic field components E_r and H_r , respectively. Then one must evaluate a double set of BSCs dependent on the radial field components [6]. During the past three decades, several methods have been developed such as quadratures [7], finite series [8], localized approximation (LA) [9,10] and integral localized approximation (ILA) [11]. Quadratures appear under two formulations, one using a 2-dimensional integrals over the polar angle θ and azimuth angle ϕ and the other using a 3-dimensional integrals over all the three spherical coordinates r , θ and ϕ . The 2-dimensional integral method is much faster than the 3-dimensional integral method because it requires one fewer integration. In the 2-dimensional integral method, the radial coordinate is localized at the specific value $kr = n + 0.5$, same as that is used in the original LA method. Here, k is the wavenumber and n is the index of partial wave. Quadra-

tures are very flexible because only the expressions for the radial components need to be changed when the nature of beam is changed. Unfortunately, the quadrature methods are very time consuming because the functions to be integrated oscillate greatly, which limits their applications. Finite-series method is much faster than quadratures in numerical calculation but extra algebraic steps are required when the nature of the beam is changed. At present, only the case of Gaussian beams has been investigated. The LA method relied on an analogy to the van de Hulst localization principle [12] and it was rigorously justified [13]. The LA method provides a very powerful tool for evaluating the BSCs efficiently and the loss of accuracy associated with the approximation is not significant in most cases. In the LA method, the radial field components E_r and H_r must be first expanded into azimuth modes and then the localization operation is made. Expanding the radial components into azimuth modes is a very tedious analytical process. As a result, the BSCs for a shaped beam are usually expressed in terms of double (or triple and even quadruple) summations of infinite series of terms depending on the characteristics of the beam [14,15], which is cumbersome to calculate and the infinite series is frequently slowly-convergent. In order to prevent from this disadvantage, the compact formulations of the BSCs are derived for a circular Gaussian beam (CGB) [16] and an elliptical Gaussian beam (EGB) [17], wherein the BSCs are expressed in terms of (modified) Bessel functions. The ILA can be viewed as a hybrid of the quadrature method and the LA because it still uses a quadrature and prescriptions from the localized approximation. It is efficient from a

* Corresponding author.

E-mail address: jqshenk@usst.edu.cn (J. Shen).

computational point of view and exhibits good properties of flexibility and stability [11,14].

The circular and elliptical Gaussian beams are usually given in their low order approximations and hence the form of the beam field is non-Maxwellian. All the methods (i.e. quadrature, finite series, LA and ILA) remodel the original beam field into a Maxwellian field in their own right. Numerical study shows that the LA method produces pseudo distribution in the reconstructed beam field [13,17,18]. The quadrature method, however, exhibits excellent fidelity to the original beam profile. In our previous work, the integration over the azimuth angle ϕ is analytically carried out and the quadrature method is simplified to 1-dimensional integration for evaluating the BSCs of a CGB [19]. As a result, the 1-dimensional quadrature method is dozens faster than the 2-dimensional one and it gets more accurate results than the LA method does. In the paper, we will extend this method to the EGB. The analytical deduction is a simple task due to the similarity between the EGB and the CGB. However, the expressions of BSCs of the EGB we obtain are much more complicated than those of the CGB. It is more difficult to implement the relevant numerical calculation because the axial asymmetry of the EGB leads to the constructive or destructive interference between the (modified) Bessel functions of different orders in the BSC-calculation. The interference depends on the eccentricity of the beam cross-section, the location of the beam center and the orientation of the beam in the coordinate system. This limits the capacity of the quadrature and LA methods for evaluating the BSCs of the EGB.

In Section 2, expressions of the BSCs of the EGB are derived in terms of 1-dimensional integration. For sake of numerical calculation, the normalized associated Legendre functions (NALF) are employed. The formulations of BSCs of the LA method, corresponding to the NALFs, are also given so that both the methods can be compared numerically. Section 3 is devoted to numerical calculations of the BSCs. The methods are checked by reconstructing the beam fields and limitations of the concerned methods are discussed in detail with examples. Conclusions are given in Section 4.

2. Formulations of the BSCs for the EGB

2.1. BSCs expressed in 2-dimensional integrations

In processing light scattering of a spherical particle in the GLMT framework, the beam field is expanded in terms of spherical wave functions. Following Barton's notation [20], the components of the electric and magnetic fields are expressed as follows:

$$\begin{cases} E_r = \frac{iE_0}{\rho^2} \sum_{n=1}^{\infty} \sum_{m=-n}^n c_n^{\text{pw}} n(n+1) A_{nm} \psi_n(\rho) \tilde{P}_n^{|m|}(\cos \theta) e^{im\phi} \\ E_\theta = \frac{iE_0}{\rho} \sum_{n=1}^{\infty} \sum_{m=-n}^n c_n^{\text{pw}} \left\{ A_{nm} \psi'_n(\rho) \tilde{\tau}_n^{|m|} - B_{nm} \psi_n(\rho) m \tilde{\pi}_n^{|m|} \right\} e^{im\phi} \\ E_\phi = -\frac{E_0}{\rho} \sum_{n=1}^{\infty} \sum_{m=-n}^n c_n^{\text{pw}} \left\{ A_{nm} \psi'_n(\rho) m \tilde{\pi}_n^{|m|} - B_{nm} \psi_n(\rho) \tilde{\tau}_n^{|m|} \right\} e^{im\phi} \end{cases} \quad (1)$$

$$\begin{cases} H_r = \frac{iH_0}{\rho^2} \sum_{n=1}^{\infty} \sum_{m=-n}^n c_n^{\text{pw}} n(n+1) B_{nm} \psi_n(\rho) \tilde{P}_n^{|m|}(\cos \theta) e^{im\phi} \\ H_\theta = \frac{iH_0}{\rho} \sum_{n=1}^{\infty} \sum_{m=-n}^n c_n^{\text{pw}} \left\{ B_{nm} \psi'_n(\rho) \tilde{\tau}_n^{|m|} + A_{nm} \psi_n(\rho) m \tilde{\pi}_n^{|m|} \right\} e^{im\phi} \\ H_\phi = -\frac{H_0}{\rho} \sum_{n=1}^{\infty} \sum_{m=-n}^n c_n^{\text{pw}} \left\{ B_{nm} \psi'_n(\rho) m \tilde{\pi}_n^{|m|} + A_{nm} \psi_n(\rho) \tilde{\tau}_n^{|m|} \right\} e^{im\phi} \end{cases} \quad (2)$$

where $\rho = kr$ is the dimensionless radius; k is the wavenumber of the light in the medium; (r, θ, ϕ) are the radius, polar and azimuth angles in the spherical coordinate system (as shown in

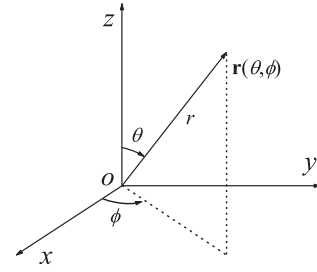


Fig. 1. Geometrical scheme of the coordinates.

Fig. 1); the weighting coefficients of the spherical wave functions, i.e. A_{nm} and B_{nm} , describe the characteristics of the beam and thus are called as the beam shape coefficients (BSC); the factor $c_n^{\text{pw}} = i^n (2n+1)/2n(n+1)$ also appears in the expansion of a plane wave (the superscript pw stands for plane wave); E_0 and H_0 are the field amplitudes at a chosen position, satisfying the relation $H_0 = (k/\omega\mu)E_0$; ω is the angular frequency and μ is the permeability; the time convention $e^{-i\omega t}$ is omitted; $\psi_n(\rho)$ is the first kind Riccati-Bessel function; $\tilde{P}_n^m(\cos \theta)$ is the NALF of degree n and order m . According to Ferrer's definition, it is given as

$$\tilde{P}_n^m(x) = \sqrt{\frac{(2n+1)(n-m)!}{2(n+m)!}} (1-x^2)^{\frac{m}{2}} \frac{1}{2^n n!} \frac{d^{m+n}}{dx^{m+n}} (x^2-1)^n \quad (3)$$

in which $x = \cos \theta$. Correspondingly, $\tilde{\pi}_n^m(\theta) = \tilde{P}_n^m(\cos \theta)/\sin \theta$ and $\tilde{\tau}_n^m(\theta) = d\tilde{P}_n^m(\cos \theta)/d\theta$ are the angular-dependent functions.

By using the orthogonality of spherical harmonics, the BSCs A_{nm} and B_{nm} can be obtained from the radial components of the beam E_r and H_r and their expansions in the spherical coordinates expressed in Eqs. (1) and (2).

$$\begin{pmatrix} A_{nm} \\ B_{nm} \end{pmatrix} = \frac{(-i)^{n+1}}{\pi (2n+1)} \frac{\rho^2}{\psi_n(\rho)} \int_0^\pi d\theta \sin \theta \tilde{P}_n^{|m|}(\cos \theta) \times \int_0^{2\pi} d\phi e^{-im\phi} \begin{pmatrix} E_r/E_0 \\ H_r/H_0 \end{pmatrix} \quad (4)$$

The BSCs A_{nm} and B_{nm} are expressed in the 2-dimensional integrations, one over the polar angle and the other over the azimuth angle. If the beam field to be expanded is an exact solution of Maxwell's equations, the BSCs describe the given beam perfectly. Contrarily, if the given beam is non-Maxwellian, the determination of the BSCs produces a remodeling of the beam, which depends on the way for evaluating them.

In the negative time convention $e^{-i\omega t}$, the radial field components of the EGB are approximated to [21]:

$$\begin{cases} E_r = E_0 \psi_0^{\text{sh}} [\cos \phi \sin \theta - 2Q_x s_x^2 \cos \theta (\rho \cos \phi \sin \theta - X_0)] e^{i\rho \cos \theta - iZ_0} \\ H_r = H_0 \psi_0^{\text{sh}} [\sin \phi \sin \theta - 2Q_y s_y^2 \cos \theta (\rho \sin \phi \sin \theta - Y_0)] e^{i\rho \cos \theta - iZ_0} \end{cases} \quad (5)$$

with

$$\psi_0^{\text{sh}} = -i\sqrt{Q_x Q_y} e^{iQ_x s_x^2 (\rho \sin \theta \cos \phi - X_0)^2 + iQ_y s_y^2 (\rho \sin \theta \sin \phi - Y_0)^2} \quad (6)$$

$$\begin{cases} Q_x = [2s_x^2 (\rho \cos \theta - Z_0) - i]^{-1} \\ Q_y = [2s_y^2 (\rho \cos \theta - Z_0) - i]^{-1} \end{cases} \quad (7)$$

where s_x and s_y are the transverse beam confinement parameters in x - and y -directions, defined as $s_x = 1/k\omega_{0x}$ and $s_y = 1/k\omega_{0y}$; ω_{0x} and ω_{0y} are the corresponding beam waist radii; (x_0, y_0, z_0) are the coordinates of the center of the beam waist in the Cartesian system and correspondingly $(X_0, Y_0, Z_0) = k(x_0, y_0, z_0)$ are the dimensionless coordinates. The factor ψ_0^{sh} can be further written as

a product of two factors $\psi_0^{\text{sh}} = \psi_0^{0,\text{sh}} \psi_0^{\phi,\text{sh}}$, wherein $\psi_0^{0,\text{sh}}$ is independent of the azimuth ϕ and $\psi_0^{\phi,\text{sh}}$ is dependent on ϕ .

$$\psi_0^{0,\text{sh}} = -i\sqrt{Q_x Q_y} e^{\frac{i}{2}(Q_x s_x^2 + Q_y s_y^2)} \rho^2 \sin^2 \theta + i(Q_x s_x^2 X_0^2 + Q_y s_y^2 Y_0^2) \quad (8)$$

$$\psi_0^{\phi,\text{sh}} = e^{\frac{\alpha}{2}[\exp(i2\phi) + \exp(-i2\phi)] + \beta \cos(\phi - \xi)} \quad (9)$$

where

$$\alpha = \frac{\rho^2 \sin^2 \theta}{2} (iQ_x s_x^2 - iQ_y s_y^2) \quad (10)$$

$$\beta = -i2\rho G_{xy} \sin \theta \quad (11)$$

$$\begin{cases} G_{xy} = \sqrt{(Q_x s_x^2 X_0)^2 + (Q_y s_y^2 Y_0)^2} \\ \cos \xi = Q_x s_x^2 X_0 / G_{xy} \\ \sin \xi = Q_y s_y^2 Y_0 / G_{xy} \end{cases} \quad (12)$$

Substituting Eq. (5) into Eq. (4) and after some algebra, we have

$$\begin{pmatrix} A_{nm} \\ B_{nm} \end{pmatrix} = \gamma_0 \int_0^\pi \gamma_1 \begin{pmatrix} \gamma_2^A \\ \gamma_2^B \end{pmatrix} d\theta \quad (13)$$

where the factors γ_0 , γ_1 and (γ_2^A, γ_2^B) are defined as

$$\gamma_0 = \frac{(-i)^n}{(2n+1)} \frac{\rho^2}{\psi_n(\rho)} e^{-iz_0} \quad (14)$$

$$\gamma_1 = \sin \theta \tilde{F}_n^{[m]}(\cos \theta) \sqrt{Q_x Q_y} e^{\frac{i}{2}(Q_x s_x^2 + Q_y s_y^2)} \rho^2 \sin^2 \theta + i(Q_x s_x^2 X_0^2 + Q_y s_y^2 Y_0^2) + i\rho \cos \theta \quad (15)$$

$$\begin{cases} \gamma_2^A = \sin \theta (2Q_x s_x^2 \rho \cos \theta - 1) (I_{m-1}^\phi + I_{m+1}^\phi) - 4Q_x s_x^2 X_0 \cos \theta \cdot I_m^\phi \\ \gamma_2^B = i \sin \theta (2Q_y s_y^2 \rho \cos \theta - 1) (I_{m+1}^\phi - I_{m-1}^\phi) - 4Q_y s_y^2 Y_0 \cos \theta \cdot I_m^\phi \end{cases} \quad (16)$$

where I_m^ϕ is the inner integral over the azimuth angle ϕ :

$$I_m^\phi = \frac{1}{2\pi} \int_0^{2\pi} e^{\frac{\alpha}{2}[\exp(i2\phi) + \exp(-i2\phi)] + \beta \cos(\phi - \xi) - im\phi} d\phi \quad (17)$$

The above procedure results into the formulations of the BSCs that are given in 2-dimensional integrations, in which the radius ρ is localized at $n+0.5$. The integrand of the inner integral over the azimuth angle ϕ becomes violently oscillatory when the index of azimuth mode m is high. The integrand of the outer integral over the polar angle θ consists of the NALF $\tilde{F}_n^{[m]}(\cos \theta)$ and hence is also oscillatory for high order partial waves. Therefore, numerical calculation of the BSCs by using the 2-dimensional integrations is very time-consuming. Furthermore, when the result of integration is several orders less than the integrand, it becomes very difficult to obtain the reasonable values of BSCs because the subtraction between big values may exhaust the significant digits. This happens when n and/or m are high.

2.2. Simplifying the quadrature method

Following the steps described in [17], the integral over the azimuth angle of Eq. (17) can be expressed in terms of the modified Bessel functions. To do so, the factor $\exp\{\alpha[\exp(i2\phi) + \exp(-i2\phi)]/2\}$ is first expanded into Taylor series

$$e^{\frac{\alpha}{2}[\exp(i2\phi) + \exp(-i2\phi)]} = \sum_{p=0}^{\infty} \sum_{q=0}^{\infty} \frac{(\alpha/2)^{p+q}}{p!q!} e^{i2(p-q)\phi} \quad (18)$$

and then Eq. (17) is developed into the form

$$I_m^\phi = \sum_{p=0}^{\infty} \sum_{q=0}^{\infty} \frac{(\alpha/2)^{p+q}}{p!q!} \frac{1}{2\pi} \int_0^{2\pi} d\phi e^{i(2p-2q-m)\phi + \beta \cos(\phi - \xi)} \quad (19)$$

Using the integral representation of the modified Bessel function and after some algebra, we have

$$I_m^\phi = \sum_{s=-\infty}^{\infty} I_s(\alpha) I_{m+2s}(\beta) e^{-i(m+2s)\xi} \quad (20)$$

where $I_s(\alpha)$ and $I_{m+2s}(\beta)$ are the modified Bessel functions of integer orders.

The above procedure transfers the inner integration over the azimuth angle into a summation of the modified Bessel functions and hence simplifies the 2-dimensional integrations into the 1-dimensional integration. This makes it possible to expedite the numerical calculation, because the modified Bessel functions can be numerically calculated with relevant recurrence.

Usually, the dependence of the beam field on the azimuth angle is described by triangle functions, i.e. $\sin \phi$ and $\cos \phi$. Using the identities $\sin \phi = (e^{i\phi} - e^{-i\phi})/2i$ and $\cos \phi = (e^{i\phi} + e^{-i\phi})/2$, and then expanding the ϕ -dependent terms into the Taylor series of the exponential function $e^{i\phi}$ if necessary, the integral over the azimuth angle can be expressed in terms of the (modified) Bessel functions, after some algebraic manipulation. Such are the cases of the CGB [19], the EGB [17], the Bessel beams [22,23], Gaussian-Bessel beams [24] and etc. In this way, only the integration over polar angle is required to be calculated in the BSC-calculation.

2.3. Localized approximation method

The localized approximation of the radial field components results into [9,10,15]

$$\begin{cases} \hat{G}\{E_r/E_0\} = e^{-iz_0} \tilde{\psi}_0^{0,\text{sh}} \tilde{\psi}_0^{\phi,\text{sh}} \cos \phi \\ \hat{G}\{H_r/H_0\} = e^{-iz_0} \tilde{\psi}_0^{0,\text{sh}} \tilde{\psi}_0^{\phi,\text{sh}} \sin \phi \end{cases} \quad (21)$$

where the localization operator \hat{G} in its original version carries out the following operations: (1) It converts $\rho = kr$ to $\rho_n = n + 0.5$; (2) It converts θ to $\pi/2$. After undertaking the localization operations, all the parameters defined in Eqs. (7)–(12) are denoted with a bar, i.e. \bar{Q}_x , \bar{Q}_y , $\bar{\alpha}$, $\bar{\beta}$, \bar{G}_{xy} , $\tilde{\psi}_0^{0,\text{sh}}$, $\tilde{\psi}_0^{\phi,\text{sh}}$ and $\bar{\xi}$. The BSCs are thus given as

$$\begin{pmatrix} A_{nm} \\ B_{nm} \end{pmatrix} = -\frac{Z_n^m}{\pi} \int_0^{2\pi} \left(\frac{\hat{G}\{E_r\}}{\hat{G}\{H_r\}} / E_0 \right) e^{-im\phi} d\phi \quad (22)$$

Corresponding to the NALF, the prefactor Z_n^m is given by [19]

$$Z_n^m = i^{1-|m|} (n+0.5)^{\frac{1}{2}-|m|} \sqrt{\frac{(n+|m|)!}{(n-|m|)!}} \quad (23)$$

Eq. (22) is indeed the formulation of BSCs proposed in the ILA method [11]. Following the steps introduced in the above section, it can be further simplified to the series of integer order modified Bessel functions. The eventual expressions of BSCs are obtained as

$$\begin{pmatrix} A_{n,m} \\ -iB_{n,m} \end{pmatrix} = -Z_n^m \tilde{\psi}_0^{0,\text{sh}} e^{-iz_0} \cdot \Phi_m \quad (24)$$

$$\Phi_m = \sum_{s=-\infty}^{\infty} [I_s(\bar{\alpha}) \pm I_{s+1}(\bar{\alpha})] I_{m+2s+1}(\bar{\beta}) e^{-i(m+2s+1)\bar{\xi}}$$

These expressions are equivalent to those in [17] but are more concise.

2.4. Special cases

2.4.1. Off-axis Location of a Circular Gaussian Beam

The CGB can be taken as a special case of the EGB when $\omega_{0x} = \omega_{0y} = \omega_0$. For a CGB we have $Q_x = Q_y = Q$ and thus $\alpha = 0$. Therefore, Eq. (20) is simplified to $I_m^\phi = I_m(\beta)e^{-im\xi}$ and correspondingly the factors of the integrand for evaluating the BSCs in the quadrature method (see Eqs. (15) and (16)) are given as

$$\gamma_1 = Qe^{iQs^2(\rho^2\sin^2\theta + \rho_0^2) + i\rho\cos\theta}\tilde{p}_n^{[m]}(\cos\theta)\sin\theta \quad (25)$$

$$\begin{cases} \gamma_2^A = \sin\theta(2Qs^2\rho\cos\theta - 1) \\ \quad \times [e^{-i(m+1)\xi}I_{m+1}(\beta) + e^{-i(m-1)\xi}I_{m-1}(\beta)] \\ \quad - 4Qs^2X_0\cos\theta \cdot e^{-im\xi}I_m(\beta) \\ \gamma_2^B = i\sin\theta(2Qs^2\rho\cos\theta - 1) \\ \quad \times [e^{-i(m+1)\xi}I_{m+1}(\beta) - e^{-i(m-1)\xi}I_{m-1}(\beta)] \\ \quad - 4Qs^2Y_0\cos\theta \cdot e^{-im\xi}I_m(\beta) \end{cases} \quad (26)$$

where $\rho_0^2 = X_0^2 + Y_0^2$ and $s = s_x = s_y$. Substitution of Eqs. (14), (25) and (26) into Eq. (13) leads to the same BSCs with those obtained in Eqs. (17)–(20) of [19].

Similarly, the BSCs in the LA method are obtained as

$$\begin{pmatrix} A_{n,m} \\ -iB_{n,m} \end{pmatrix} = Z_n^m i\tilde{Q}e^{i\tilde{Q}s^2(\rho_n^2 + \rho_0^2) - iZ_0} \\ \times [e^{-i(m+1)\xi}I_{m+1}(\tilde{\beta}) \pm e^{-i(m-1)\xi}I_{m-1}(\tilde{\beta})] \quad (27)$$

which are same as those given in Eqs. (28)–(30) of [19].

2.4.2. On-axis location of an Elliptical Gaussian Beam

For on-axis situation (i.e. $X_0 = Y_0 = 0$), the parameter $\beta = \tilde{\beta} = 0$ and hence we have $I_{m=2p+1}^\phi = 0$ and $I_{m=2p}^\phi = I_p(\alpha)$, where p is an integer. Therefore, the BSCs are equal to zero for all the even azimuth modes, i.e. $A_{nm} = B_{nm} = 0$ when $m = 2p$. Those BSCs of odd azimuth modes satisfy the relation $A_{n,m} = A_{n,-m}$ and $B_{n,m} = -B_{n,-m}$ where $m = 2p + 1$. In this case, the factors of the integrand for evaluating the BSCs of the quadrature method are simplified to

$$\gamma_1 = \sin\theta\tilde{p}_n^{[m]}(\cos\theta)\sqrt{Q_xQ_y}e^{\frac{i}{2}(Q_xs_x^2 + Q_ys_y^2)\rho^2\sin^2\theta + i\rho\cos\theta} \quad (28)$$

$$\begin{cases} \gamma_2^A = \sin\theta(2Q_xs_x^2\rho\cos\theta - 1)[I_{p+1}(\alpha) + I_p(\alpha)] \\ \gamma_2^B = i\sin\theta(2Q_ys_y^2\rho\cos\theta - 1)[I_{p+1}(\alpha) - I_p(\alpha)] \end{cases} \quad (29)$$

and the BSCs in the LA method are given as

$$\begin{pmatrix} A_{n,m=2p+1} \\ -iB_{n,m=2p+1} \end{pmatrix} = -Z_n^m \tilde{\psi}_0^{0,sh} e^{-iZ_0} \cdot [I_{p+1}(\tilde{\alpha}) \pm I_p(\tilde{\alpha})] \quad (30)$$

The existence of such symmetry relations above can be used to avoid calculating all the BSCs and thus expedites the numerical calculations.

3. Numerical calculation and discussion

3.1. Numerical techniques in calculation

The numerical evaluation of the BSCs in the quadrature method requires the calculation of the factors γ_0 , γ_1 and (γ_2^A, γ_2^B) , defined in Eqs. (14)–(16). Therefore, we must calculate the Riccati-Bessel function $\psi_n(\rho)$, the NALF $\tilde{p}_n^{[m]}(\cos\theta)$ and the function I_m^ϕ . For the n th partial wave, the dimensionless radius ρ is localized at $\rho_n = n + 0.5$. The methods for calculating the former two functions, i.e. $\psi_n(\rho)$ and $\tilde{p}_n^{[m]}(\cos\theta)$, are described in [19] and elsewhere. So we will focus on the calculation of I_m^ϕ .

Since the modified Bessel function $I_n(z)$ for the complex argument z is proportional to the exponential of its variable for

$\arg z < \pi/2$, the function I_m^ϕ (given in Eq. (20)) may exceed the limit of the floating number when the real parts of the variables α and β are large. In order to prevent from the numerical difficulties, I_m^ϕ is transformed into another form $\tilde{I}_m^\phi = I_m^\phi \cdot e^{-\alpha\text{sgn}(\text{Re}\alpha) - \beta\text{sgn}(\text{Re}\beta)}$. Here, $\text{Re}z$ represents the real part of z and $\text{sgn}(z)$ is the sign of the variable. With such a transformation, values of \tilde{I}_m^ϕ are restricted into a reasonable range. Thus, Eqs. (17) and (20) are rewritten as

$$\tilde{I}_m^\phi = \frac{1}{2\pi} \int_0^{2\pi} e^{\alpha[\cos(2\phi) - \text{sgn}(\text{Re}\alpha)] + \beta[\cos(\phi - \xi) - \text{sgn}(\text{Re}\beta)] - im\phi} d\phi \quad (31)$$

$$\tilde{I}_m^\phi = \sum_{s=-\infty}^{\infty} \tilde{I}_s(\alpha) \tilde{I}_{m+2s}(\beta) e^{-i(m+2s)\xi} \quad (32)$$

where $\tilde{I}_m(z) = I_m(z) \cdot e^{-z\text{sgn}(\text{Re}z)}$. Corresponding to the transformation from I_m^ϕ to \tilde{I}_m^ϕ , a compensation must be made to the factor involved in the integration, i.e. $\tilde{\gamma}_1 = \gamma_1 \cdot e^{\alpha\text{sgn}(\text{Re}\alpha) + \beta\text{sgn}(\text{Re}\beta)}$. So we have

$$\begin{aligned} \tilde{\gamma}_1 &= \sin\theta\tilde{p}_n^{[m]}(\cos\theta)\sqrt{Q_xQ_y} \cdot e^{\Omega} \\ \Omega &= \begin{cases} \alpha\text{sgn}(\text{Re}\alpha) + \frac{i}{2}(Q_xs_x^2 + Q_ys_y^2)\rho^2\sin^2\theta \\ + \beta\text{sgn}(\text{Re}\beta) + i(Q_xs_x^2X_0^2 + Q_ys_y^2Y_0^2) + i\rho\cos\theta \end{cases} \end{aligned} \quad (33)$$

When the beam is not too far away from the z -axis, the value of $\text{Re}\Omega$ is small so that $\tilde{\gamma}_1$ is restricted in a reasonable range of values. Therefore, the BSCs of the 1-dimensional integration of the GLMT can be rewritten as

$$\begin{pmatrix} A_{nm} \\ B_{nm} \end{pmatrix} = \gamma_0 \int_0^\pi \tilde{\gamma}_1 \begin{pmatrix} \tilde{\gamma}_2^A \\ \tilde{\gamma}_2^B \end{pmatrix} d\theta \quad (34)$$

together with

$$\begin{cases} \tilde{\gamma}_2^A = \sin\theta(2Q_xs_x^2\rho\cos\theta - 1)(\tilde{I}_{m-1}^\phi + \tilde{I}_{m+1}^\phi) - 4Q_xs_x^2X_0\cos\theta \cdot \tilde{I}_m^\phi \\ \tilde{\gamma}_2^B = i\sin\theta(2Q_ys_y^2\rho\cos\theta - 1)(\tilde{I}_{m-1}^\phi - \tilde{I}_{m+1}^\phi) - 4Q_ys_y^2Y_0\cos\theta \cdot \tilde{I}_m^\phi \end{cases} \quad (35)$$

In the similar way, the BSCs of the LA method are modified to

$$\begin{pmatrix} A_{n,m} \\ -iB_{n,m} \end{pmatrix} = -Z_n^m \tilde{\psi}_0^{0,sh} e^{-iZ_0} \tilde{\Phi}_m \\ \tilde{\Phi}_m = \sum_{s=-\infty}^{\infty} [\tilde{I}_s(\tilde{\alpha}) \pm \tilde{I}_{s+1}(\tilde{\alpha})] \tilde{I}_{m+2s+1}(\tilde{\beta}) e^{-i(m+2s+1)\xi} \quad (36)$$

where $\tilde{\psi}_0^{0,sh}$ is given as

$$\begin{aligned} \tilde{\psi}_0^{0,sh} &= -i\sqrt{Q_xQ_y}e^{\tilde{\Omega}} \\ \tilde{\Omega} &= \tilde{\alpha}\text{sgn}(\text{Re}\tilde{\alpha}) + \tilde{\beta} \cdot \text{sgn}(\text{Re}\tilde{\beta}) \\ &\quad + \frac{i}{2}(\tilde{Q}_xs_x^2 + \tilde{Q}_ys_y^2)\rho_n^2 + i(\tilde{Q}_xs_x^2X_0^2 + \tilde{Q}_ys_y^2Y_0^2) \end{aligned} \quad (37)$$

Here, $\tilde{\Omega}$ is the special case of Ω at $\theta = \pi/2$ and similarly we have $\tilde{\Phi}_m = \tilde{I}_{m+1}^\phi \pm \tilde{I}_{m-1}^\phi$ for $\theta = \pi/2$.

3.2. Superiority of 1-dimensional quadrature to 2-dimensional quadrature

Since the function \tilde{I}_m^ϕ is expressed in terms of an integral over the azimuth angle ϕ (see Eq. (31)) or a sum of infinite terms related with the modified Bessel functions (see Eq. (32)), there are two methods for calculating \tilde{I}_m^ϕ : one uses the quadrature method and the other is the series method involving the calculation of modified Bessel functions.

The integration of \tilde{I}_m^ϕ (see Eq. (31)) can be implemented by using Romberg method combined the composite trapezoidal rule.

Table 1
Comparison of numerical results and CPU time in calculating \tilde{I}_m^ϕ .

(n, m)	Desired accuracy	Quadrature method, Eq. (31) (s)		Series method, Eq. (32) (s)		Ratio t_1/t_2
		result	CPU time t_1 (μ s)	result	CPU time t_2 (μ s)	
(28,1)	10^{-5}	(1.776576e-1, -2.612723e-2)	30.9	(1.776577e-1, -2.612724e-2)	63.3	0.49
	10^{-10}	(1.776577e-1, -2.612724e-2)	113			1.78
(28,5)	10^{-5}	(-2.536743e-6, 4.491014e-5)	127	(-2.536090e-6, 4.490991e-5)	64.1	1.98
	10^{-10}	(-2.536090e-6, 4.490991e-5)	293			4.58
(28,10)	10^{-5}	(8.076819e-11, 4.156075e-10)	280	(3.416834e-10, 3.903496e-10)	63.3	4.42
	10^{-10}	(3.416834e-10, 3.903496e-10)	586			9.26
(28,15)	10^{-5}	(-1.493460e-10, 1.117066e-11)	435	(1.846294e-15, -3.638928e-16)	69.1	6.29
	10^{-10}	(1.750962e-15, -3.641625e-16)	932			13.5

The integrand consists of the factor $e^{-im\phi}$ and hence becomes violently oscillatory when the azimuth index is high. Therefore, the numerical integration is performed by subdividing the interval into several equidistant ones, according to the azimuth index. The CPU time for the integration depends on both the oscillations of the integrand and the desired accuracy.

The use of Eq. (32) for evaluating \tilde{I}_m^ϕ requires calculating a double set of the modified Bessel functions $\tilde{I}_s(\alpha)$ and $\tilde{I}_{m+2s}(\beta)$. The summation of the series can be truncated, depending on their variables α and β . The criteria for the lower and upper limits of the integer s can be easily evaluated because both the functions $\tilde{I}_s(\alpha)$ and $\tilde{I}_{m+2s}(\beta)$ are successively descending when their orders deviate from zero. Therefore, the CPU time consumed in numerical calculation is determined by the truncating conditions.

The results of \tilde{I}_m^ϕ and the corresponding CPU times of the quadrature method and the series method are compared for a fixed partial index $n=28$, as shown in Table 1. The involved parameters are $\omega_{0x}=2\text{ }\mu\text{m}$, $\omega_{0y}=6\text{ }\mu\text{m}$, $\lambda=0.6328\text{ }\mu\text{m}$, $\theta=0.3\text{rad}$, $x_0=y_0=2\text{ }\mu\text{m}$ and $z_0=0$. It can be seen that, for very low azimuth modes such as $m=1$, reliable results can be obtained by the quadrature method with a low desired accuracy, and the method is fast. For high azimuth modes (e.g. $m=5$ & 10), the desired accuracy of the integration must be improved so as to obtain reliable results. When the azimuth is very high (i.e. $m \geq 15$), the value of \tilde{I}_m^ϕ is so small (say less than 10^{-16}) that the quadrature method is unable to get reliable results. Nonetheless, in all these cases the series method can get reliable results and it requires much less CPU time than the quadrature method.

In the evaluation of BSCs of the GLMT quadrature method, the 2-dimensional quadrature method requires the outer integration over the polar angle and the inner integration over the azimuth angle (see Eq. (31)) but in the 1-dimensional quadrature method the inner integration is replaced by the series method (see Eq. (32)). The essential difference between the 1-dimensional quadrature method and the 2-dimensional one of the GLMT is the methods for calculating the factor \tilde{I}_m^ϕ . Since the series method is much faster and more reliable than the numerical integration, the 1-dimensional quadrature method of the GLMT improves the numerical calculation in both the numerical reliability and computation efficiency.

3.3. BSC calculation and beam reconstruction

The BSCs are computed with the 1-dimensional quadrature method (Eqs. (34) and (35)) and with the LA method (Eqs. (36) and (37)) too. The electric field of the beam is reconstructed from the calculated BSCs. Then the proposed numerical method for evaluating the BSCs is verified by comparing the reconstructed beam field with the given beam.

The integrands in Eq. (34) oscillate, depending closely on the partial wave order n and azimuth index m , as illustrated in Fig. 2. The beam parameters are $\omega_{0x}=2.5\text{ }\mu\text{m}$, $\omega_{0y}=5\text{ }\mu\text{m}$, $\lambda=0.6328\text{ }\mu\text{m}$,

$x_0=6\text{ }\mu\text{m}$, $y_0=4\text{ }\mu\text{m}$ and $z_0=0$. It can be seen that the integrand oscillates uniformly in the interval $[0, \pi]$ and the frequency of oscillations increases along with the increase of the partial wave order n , because of the NALF $\tilde{P}_n^{[m]}(\cos\theta)$. For a fixed low azimuth index (e.g. $m=0$), the amplitude of the integrand varies in the way mainly determined by the variation of $\tilde{\gamma}_1$. Along with the increase of partial wave order n , the integrand increases, reaches the maximum and then turns to decrease, as shown in Figs. 2a, 2c and 2e for $m=0$.

In the evaluation of the BSCs with 1-dimensional GLMT quadrature method, Romberg method combined with the composite trapezoidal rule is employed. The numerical calculation is executed using the double-precision VC++6.0 codes on a personal computer powered by a 3.2GHz CPU. Fig. 3 shows the dependence of the BSCs $|A_{nm}|$ on the partial wave order n and the azimuth index m . The parameters of the EGB are same as those of Fig. 2. The $|A_{n,0}|$ increases in the range of small partial wave orders, reaches the maximum at $n \approx 71$, and then turns to decrease. The maximum $|A_{n,0}|$ corresponds to the partial wave which is mainly determined by the separation between the beam center and the z -axis (i.e. $\rho_0 = k\sqrt{x_0^2 + y_0^2} \approx 71.6$) [18]. Fig. 3b shows that, when the azimuth index increases, the BSC decreases at the rate depending on the partial wave order. Visible difference between the results of the quadrature and LA methods is found for high partial waves and/or high azimuth modes, as shown in Fig. 3b.

In order to reconstruct the beam field, we must calculate all the required BSCs in a wide range of partial wave orders and azimuth indices. From Fig. 3, we find that the maximum of BSCs corresponds to the partial waves $n \approx \rho_0$ and the azimuth modes $|m| \leq 1$. The value of the maximal BSC typically ranges from 0.1 to 10. Therefore, with a desired accuracy, it is easy to truncate the partial wave order and the azimuth index in the numerical calculation.

The beam field is reconstructed by using the BSCs that are calculated with the quadrature and LA methods, which is depicted by the curved surfaces in Fig. 4. It can be seen from Fig. 4a that the quadrature method reproduces the beam field satisfactorily in the region $|\mathbf{E}_{\text{giv}}(\mathbf{r})| \geq 10^{-7}$. Here, the subscript giv represents the given beam. Outside of the region, the reconstructed field is dominated by a background whose level is about 10^{-8} . The background is caused by the truncations of the partial waves and the azimuth modes, and also the round-off errors produced in the integration. The LA method reconstructs the intended beam profile in the region $|\mathbf{E}_{\text{giv}}(\mathbf{r})| \geq 10^{-7}$, and the background is a little lower than that of the quadrature method. Apart from the intended beam peak, the LA method produces an axially symmetric doughnut-like pseudo-distribution which is about 10^{-5} high. The relevant explanation of the pseudo-distribution is given in [19].

In order to evaluate the fidelity of the reconstructed beam field to the given one, we calculate the average of the relative errors at the coordinates where the magnitude of the given field keeps

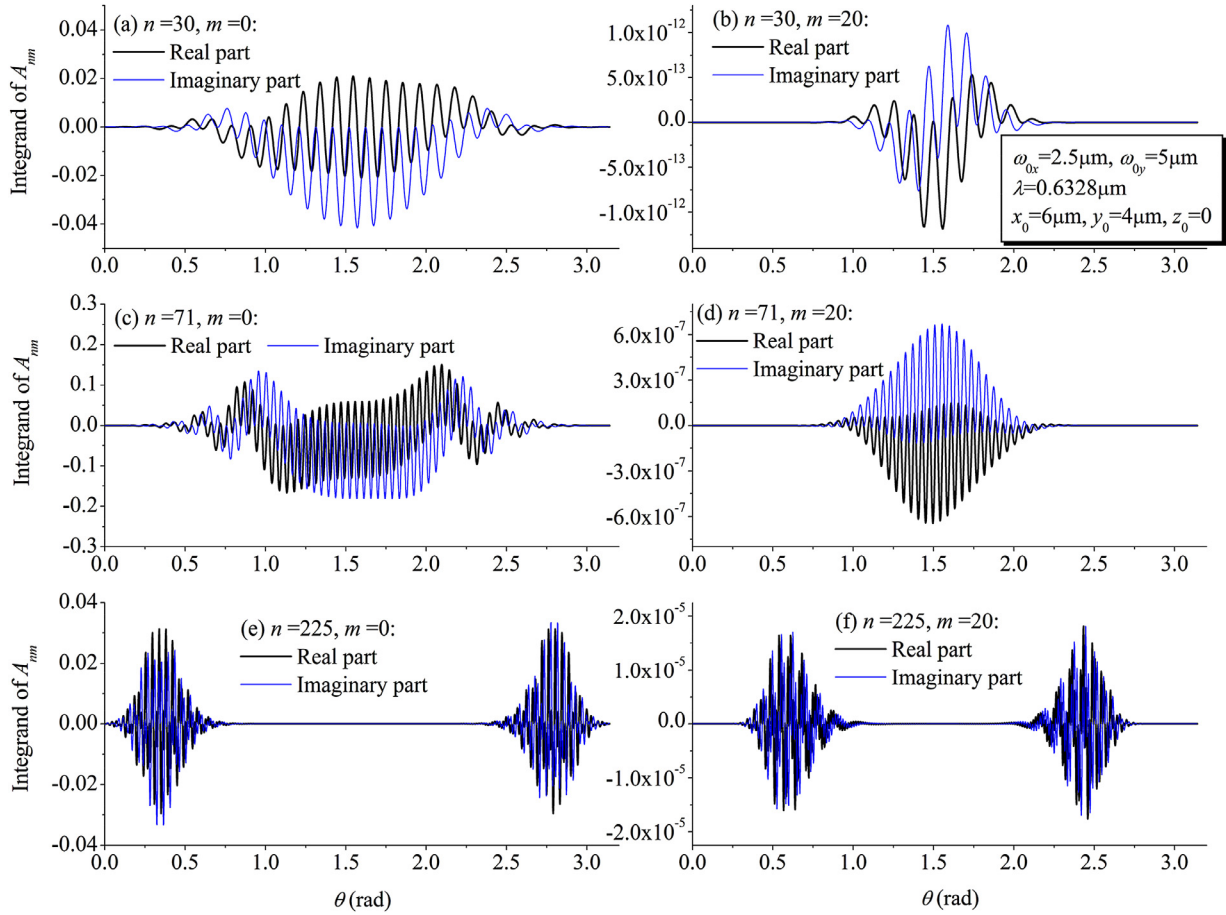


Fig. 2. Numerical results of the integrands for different partial wave orders and azimuth indices: (a) $n=30, m=0$; (b) $n=30, m=20$; (c) $n=71, m=0$; (d) $n=71, m=20$; (e) $n=225, m=0$; (f) $n=225, m=20$.

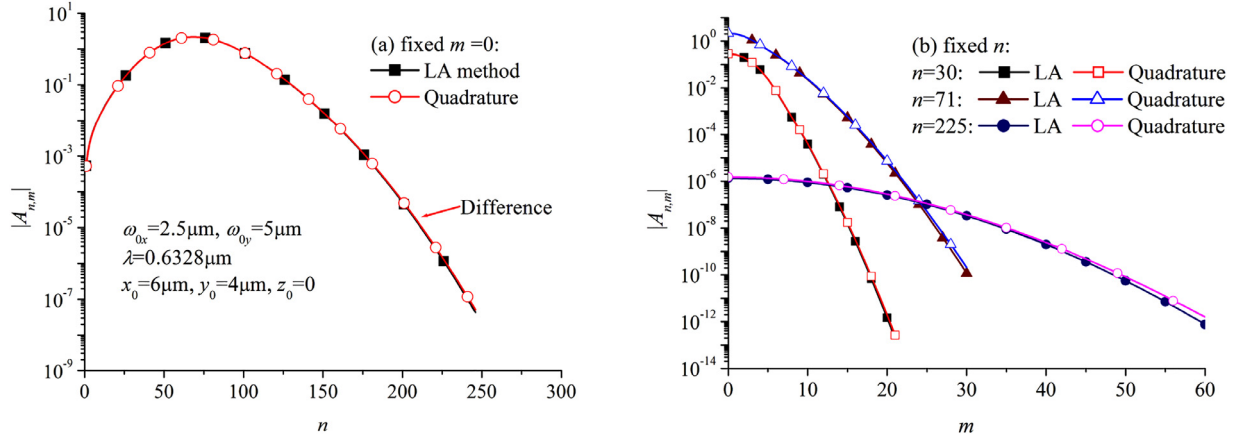


Fig. 3. numerical results of BSCs calculated with the quadrature and the LA methods: (a) dependence of BSCs on partial wave order; (b) dependence of BSCs on azimuth index. The beam parameters are same as those of Fig. 2.

unchanged. The average error is defined as

$$\bar{\varepsilon} = \frac{1}{N} \sum_{i=1}^N |1 - \mathbf{E}_{\text{rec}}(\mathbf{r}_i) / \mathbf{E}_{\text{giv}}(\mathbf{r}_i)| \quad (38)$$

Here, $\mathbf{E}_{\text{rec}}(\mathbf{r}_i)$ and $\mathbf{E}_{\text{giv}}(\mathbf{r}_i)$ represent the reconstructed and the given beam fields respectively; \mathbf{r}_i is the coordinates of the i th point on the elliptic curve

$$|\mathbf{E}_{\text{giv}}(\mathbf{r}_i)| = e^{-[(x_i - x_0)/\omega_{0x}]^2 - [(y_i - y_0)/\omega_{0y}]^2} = \text{const} \quad (39)$$

The N points involved in averaging are uniformly distributed on the ellipse. Numerical results of the average error are shown in Fig. 5. The error grows up gradually when the amplitude of the field becomes low. The beam field reconstructed by the quadrature technique agrees better with the given one than that of the LA method.

The CPU time for evaluating the BSCs A_{nm} and B_{nm} of a certain partial wave and a certain azimuth mode is listed in Table 2, corresponding to the beam parameters given in Fig. 2. It can be seen that the high partial wave and/or the high azimuth mode re-

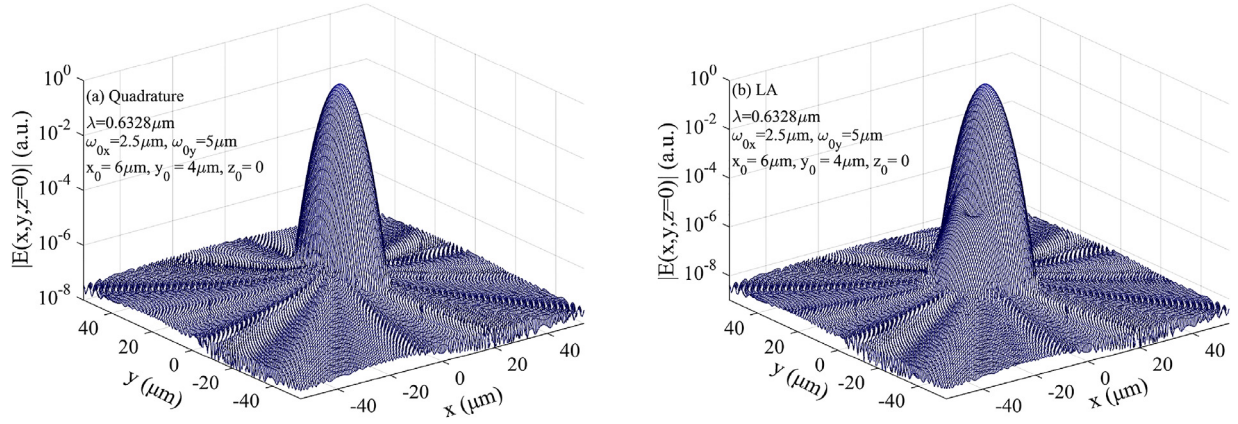


Fig. 4. Beam fields in the plane $z=0$ reconstructed by (a) the 1-dimensional integration method and (b) the LA method. The beam parameters are same as those of Fig. 2. The BSCs are calculated for orders $n \in [1, 286]$.

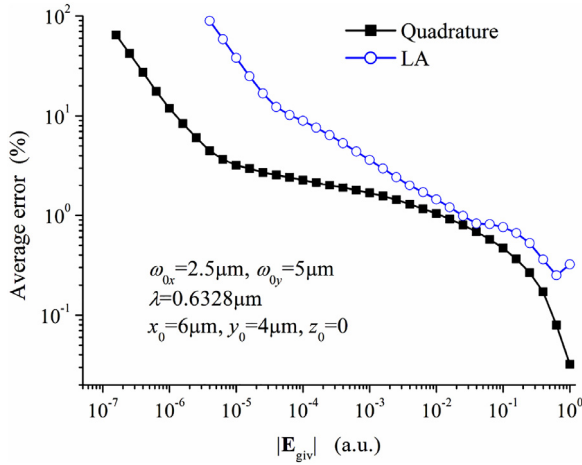


Fig. 5. Average errors of the beam fields reconstructed by the 1-dimensional integration method and the LA method. The beam parameters are same as those of Fig. 2.

Table 2
CPU time required for numerical calculation of BSC with 1-dimensional integration.

(n, m)	CPU time (μ s)	(n, m)	CPU time (μ s)
(30, 0)	57.0	(30, 20)	69.6
(71, 0)	78.9	(71, 20)	88.4
(225, 0)	180	(225, 20)	184

quires more CPU time, due to the stronger oscillations of the integrand. For evaluating all the BSCs required in the beam reconstruction, the 1-dimensional integration method takes 25.9 h but the LA method takes about 10 s only.

The CPU time of the quadrature method for evaluating the BSCs of an EGB depends on the beam confinement parameters. If the beam is very elliptical (i.e. $\omega_{0x} \gg \omega_{0y}$ or $\omega_{0x} \ll \omega_{0y}$), then more CPU time is required because more terms should be calculated for evaluating \tilde{I}_m^ϕ . For example, when the beam waist radius ω_{0y} increases from 2 μ m to 7 μ m at a fixed step $\Delta\omega_{0y} = 1$ μ m and meanwhile the other beam parameters $\omega_{0x} = 2$ μ m, $\lambda = 0.6328$ μ m, $x_0 = 4$ μ m and $y_0 = z_0 = 0$ are kept unchanged, the CPU time for evaluating all the BSCs with the 1-dimensional quadrature method is 0.15, 0.94, 4.7, 10.5, 17.2 and 26.5 h respectively. The CPU time increases in the similar way if we keep the other parameters unchanged but increase ω_{0x} gradually.

Besides, the CPU time of the quadrature method for evaluating the BSCs of an EGB also depends on the departure of the beam center from the z -axis. When the beam center departs more far away from the z -axis, the BSCs of higher partial waves should be calculated and hence more CPU time is required. For example, we fix the beam parameters $\omega_{0x} = 5$ μ m, $\omega_{0y} = 2$ μ m, $\lambda = 0.6328$ μ m and $y_0 = z_0 = 0$, and let the coordinate x_0 changes from 0 to 16 μ m at a fixed step $\Delta x_0 = 4$ μ m, the CPU time is 1.1, 7.1, 12.1, 19.3 and 30.1 h, respectively.

3.4. Limitations in numerical computation

In some cases, both the quadrature method and the LA method fail to calculate the BSCs of high partial waves correctly. Fig. 6 shows the numerical results of BSCs $|A_{nm}|$ for $m=1$, wherein the beam parameters are $\lambda = 0.6328$ μ m, $\omega_{0x} = 2$ μ m, $\omega_{0y} = 6$ μ m, $x_0 = y_0 = 5.5$ μ m and $z_0 = 0$. As depicted in Fig. 6a, the BSCs of high partial waves rapidly increase, i.e. for $n > 200$ in the quadrature method and for $n > 180$ in the LA method. By comparing the integrand of A_{nm} of Fig. 6b with that of Fig. 2e, we find that there is an additional peak in the interval close to the polar angle $\theta = \pi/2$. This peak results from the round-off errors in the \tilde{I}_m^ϕ calculation. As defined in Eq. (32), the factors \tilde{I}_m^ϕ is a sum of series of the modified Bessel functions. This indicates that the result of summation may be the constructive or destructive interference of all the involved terms, depending on the parameters α , β and ξ . With the beam parameters given in Fig. 6, the destructive interference occurs for high partial waves. When $n > 200$ the result of \tilde{I}_m^ϕ is 15 orders less than the maximum of a single term so that all the significant digits of the double-precision are lost in the numerical calculation. Since the integrand is a product of the factors $\tilde{\gamma}_1$ and $(\tilde{\gamma}_2^A, \tilde{\gamma}_2^B)$ wherein the latter factors are linear combinations of \tilde{I}_m^ϕ , a pseudo peak is produced in the integrand in the vicinity of $\theta = \pi/2$. The pseudo peak is very strong because $\tilde{\gamma}_1$ is very large in this range of polar angles. This leads to the incorrect results of the BSCs for high partial waves in the quadrature method. The situation of the LA method is quite similar to that of quadrature method, because the BSC calculation with the LA method depends directly on the calculation of $\tilde{\Phi}_m$ which is equal to $\tilde{I}_{m+1}^\phi \pm \tilde{I}_{m-1}^\phi$ at $\theta = \pi/2$ (see Eq. (36)).

Using the above calculated BSCs, the beam fields are reconstructed. The incorrect values of BSCs, i.e. those of $n \geq 180$ in the LA method and those of $n \geq 200$ in the quadrature method, are excluded in the beam field reconstruction. As a result, only part of the beam is reproduced accurately, as shown in Fig. 7. The average errors of the reconstructed field at $|E_{giv}| = 10^{-4}$ are 8.5% (quadra-

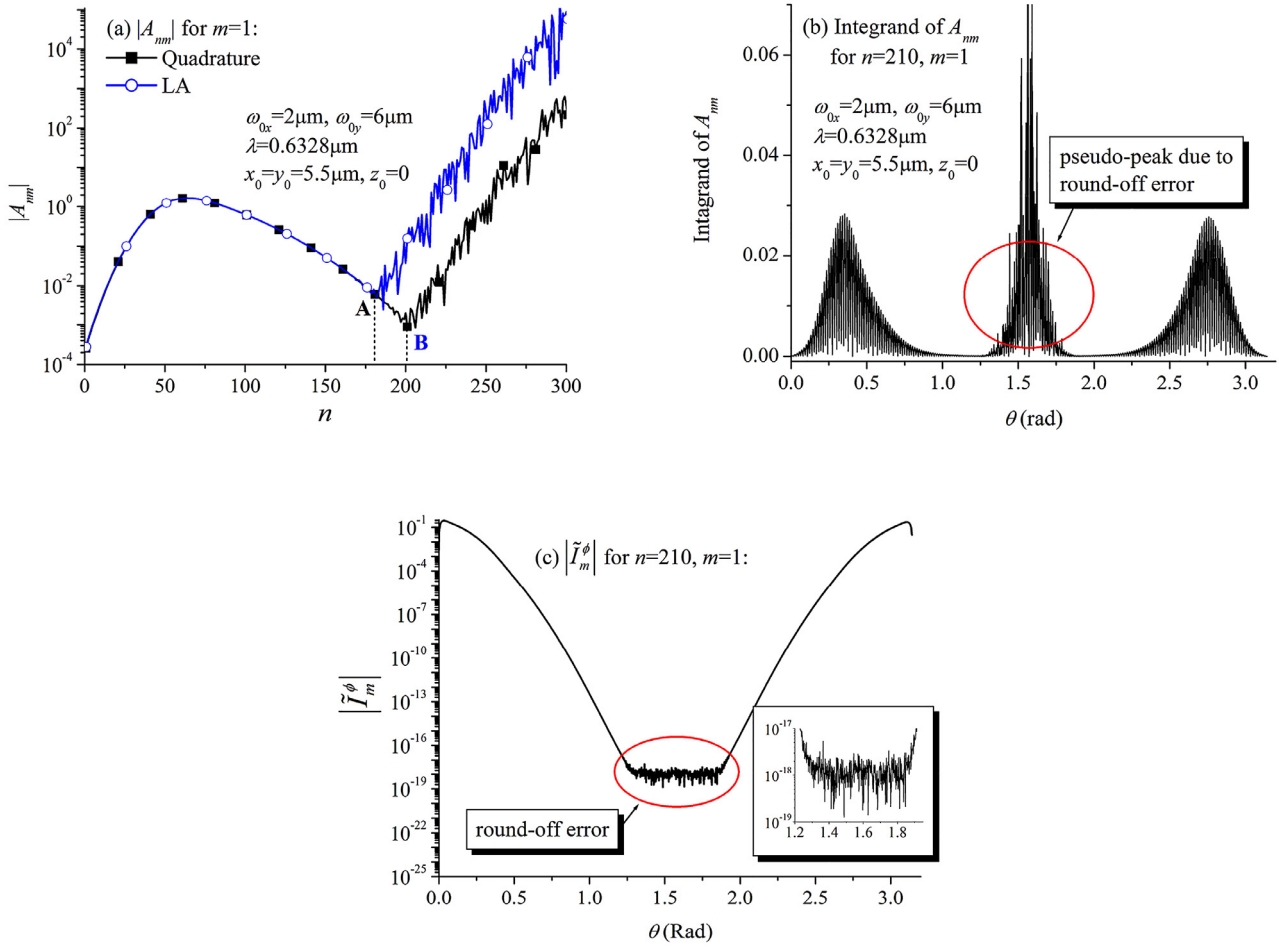


Fig. 6. Unreliable results of BSCs for high partial waves. (a) extraordinary behavior of BSCs; (b) pseudo peak of the integrand of A_{nm} ; (c) round-off errors cause by destructive interference in \tilde{I}_m^ϕ calculation.

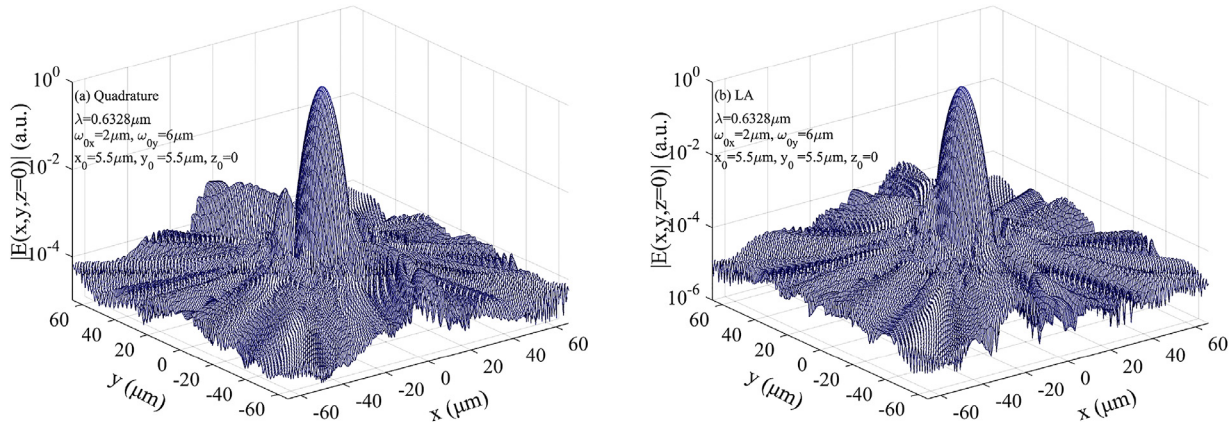


Fig. 7. Beam fields reconstructed with the BSCs calculated by: (a) the quadrature method for $n \in [1, 179]$; (b) the LA method for $n \in [1, 199]$. The beam parameters are same as those in Fig. 6.

ture) and 19% (LA) respectively. The background outside of the region is about $|\mathbf{E}_{\text{rec}}| \in [10^{-6}, 10^{-3}]$.

Further numerical calculations of the BSCs are performed with the same beam parameters shown in Fig. 6 but with different coordinates of the beam center (x_0, y_0) . Let $x_0 = r_0 \sin \delta_0$ and $y_0 = r_0 \cos \delta_0$, wherein r_0 is the transverse distance of the beam center from the z -axis and δ_0 represents the angle between the

major axis of the beam cross section and the radial vector of the beam center (i.e. $\mathbf{r}_0 = x_0 \mathbf{e}_x + y_0 \mathbf{e}_y$). Fig. 8a shows the results of BSCs $|A_{n,1}|$, where $r_0 = 7.78 \mu\text{m}$ and δ_0 varies from 0 to 90°, and Fig. 8b illustrates the location of the beam center in the xy -plane. It can be seen that the quadrature method is able to calculate the BSCs successfully for small values of δ_0 . However, the capacity of quadrature method becomes worse gradually when δ_0 increases.

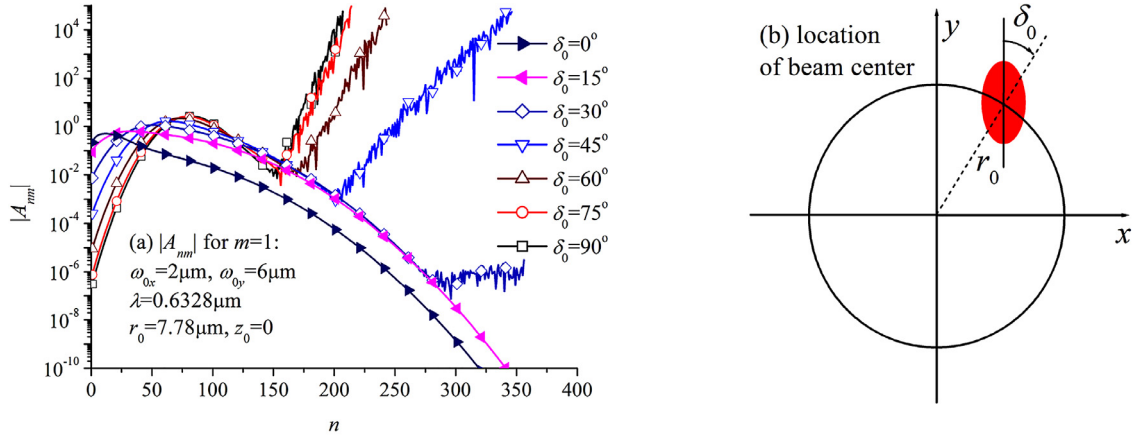


Fig. 8. Numerical results of BSCs $A_{n,1}$ of the EGB for different angles δ_0 . (a) BSCs $A_{n,1}$; (b) location of the beam center in xy -plane.

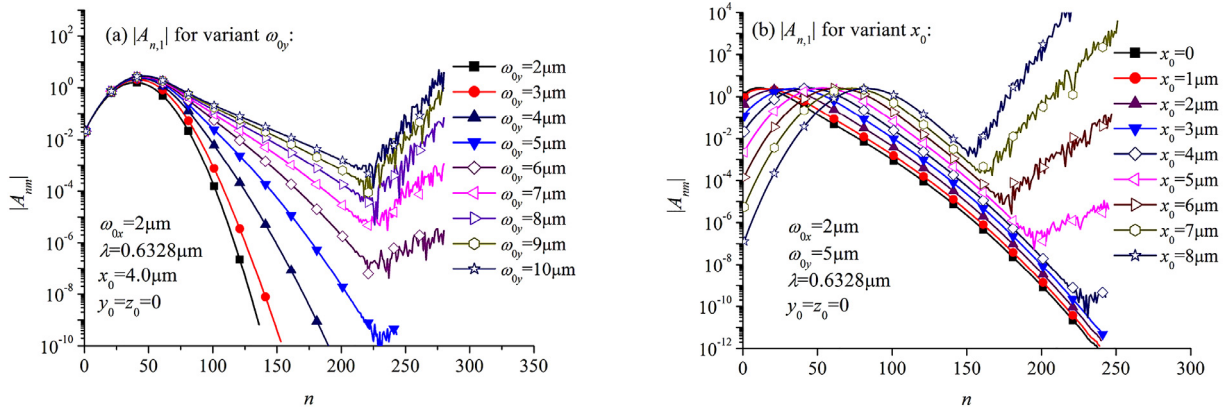


Fig. 9. Numerical results of BSCs $A_{n,1}$ of the EGB: (a) for different eccentricity; (b) for different separation between the beam center and the z -axis.

The worst situation appears at $\delta_0=90^\circ$. The numerical difficulty is once again due to the destructive interference of the terms in the calculation of \tilde{I}_m^ϕ . As can be seen from Eq. (20) or Eq. (32), the phases of the terms are decided mainly by the parameter ξ which depends closely on δ_0 . Therefore, the variation of δ_0 has strong influence on the \tilde{I}_m^ϕ calculation. When $\delta_0 \approx 90^\circ$, most of the significant digits of \tilde{I}_m^ϕ are lost and meanwhile the value of $\tilde{\gamma}_1$ (or Ω) is very large in the vicinity of $\theta = \pi/2$. As the result of this, a strong pseudo peak of the integrand is formed. The situation is quite similar with what is shown in Fig. 6b. On the contrary, when $\delta_0 \approx 0^\circ$, the factor \tilde{I}_m^ϕ can be calculated without loss of significant digits and meanwhile the value of $\tilde{\gamma}_1$ (or Ω) is very small in the vicinity of $\theta = \pi/2$. Therefore, the integrand is calculated very accurately and hence reliable results of BSCs can be acquired.

The \tilde{I}_m^ϕ calculation also depends on the parameters α and β very closely. When these parameters increases, the modified Bessel functions increase rapidly and so do the terms in the \tilde{I}_m^ϕ calculation. Therefore, the significant digits of \tilde{I}_m^ϕ may be lost very easily when the destructive interference occurs. From Eqs. (10) and (11), we know that the parameters α and β are determined by several factors, including the departure of the beam center from the z -axis r_0 , the beam waist radii (ω_{0x}, ω_{0y}), the partial wave order n and the polar angle θ . In Fig. 9a, the beam center is fixed at $x_0=4\mu\text{m}$ and $y_0=z_0=0$. The beam waist radius along the x -direction is fixed at $\omega_{0x}=2\mu\text{m}$ but that of the y -direction increases from $\omega_{0y}=2\mu\text{m}$ to $10\mu\text{m}$. In all the cases, we have $\delta_0=90^\circ$. It can be seen that, for those $\omega_{0y} \geq 5\mu\text{m}$, the numerical difficulty appears for orders

$n > 210$. In Fig. 9b, all the beam parameters keep unchanged but the beam center moves from $x_0=0$ to $x_0=8\mu\text{m}$ on the x -axis. Along with the movement of the beam, $|A_{n,1}|$ shifts outward correspondingly. Numerical difficulty appears when the beam center is far away from the z -axis (say $x_0 > 4\mu\text{m}$). The special case of $\omega_{0y}=2\mu\text{m}$ in Fig. 9a corresponds to the CGB, and that of $x_0=0$ in Fig. 9b corresponds to the on-axis location of the EGB. It was discussed in Section 2.4 that, in these special cases, the function \tilde{I}_m^ϕ (or \tilde{I}_m^ϕ) contains one term only and hence there is no interference in the numerical calculation. When the parameter ω_{0y} in Fig. 9a (or x_0 in Fig. 9b) increases gradually, more and more terms are required for calculating \tilde{I}_m^ϕ . As a result of this, the destructive interference becomes increasingly serious, which causes the loss of significant digits and the failure of BSC calculation.

Unfortunately, a quantitative description on the limitations of the 1-dimensional quadrature method and the LA method is still unavailable because of the complex dependence of the factor \tilde{I}_m^ϕ on the parameters α , β and ξ , and the dependence of these mediate parameters on the beam waist radii (ω_{0x}, ω_{0y}) and the beam center coordinates (x_0, y_0, z_0). Nevertheless, the numerical results in this paper and those in [25] reveal that reliable results of BSCs can be obtained by using the quadrature and/or the LA methods if the beam parameters satisfy the relations $(x_0/\omega_{0x})^2 + (y_0/\omega_{0y})^2 < 4$ and $0.1 \leq \omega_{0x}/\omega_{0y} \leq 10$ for $z_0=0$. It should be noted that, though all the numerical examples are given for $z_0=0$, the relevant discussions can be easily extended to $z_0 \neq 0$. To summarize qualitatively, numerical difficulty of the BSC calculation of an EGB in the

quadrature and the LA methods appears when the following conditions are satisfied simultaneously: (a) the radial vector \mathbf{r}_0 is not parallel to the major axis of the beam cross section; (b) the beam center is distant from the z-axis; (c) the eccentricity of the beam cross section is large (i.e. $\omega_{0x} \gg \omega_{0y}$ or $\omega_{0x} \ll \omega_{0y}$).

4. Conclusions

In this work, we derived the formulations for evaluating the BSCs of an EGB in the GLMT framework. The BSCs are expressed in terms of the 1-dimensional integration. The NALFs are employed so as to avoid the difficulties in numerical computation. Expressions of BSCs of the LA method are also given for comparison. Numerical study shows that the 1-dimensional integration of the quadrature method is in average dozens faster than the 2-dimensional integrations.

The calculated BSCs are used for reconstructing the beam field. The fidelity of the reproduced field to the given one is estimated by defining an average error at a certain level of the given field. It is found that the quadrature method can reconstruct the field satisfactorily in the region $|\mathbf{E}_{\text{giv}}(\mathbf{r})| \geq 10^{-7}$ and the average error increases gradually when the level of the given field decreases. The LA method produces the intended beam distribution together with an axially symmetric doughnut-like pseudo-distribution. The average error of the LA method is larger than that of the quadrature method.

The CPU time for evaluating the BSCs of the quadrature method depends on both the beam profile and the location of the beam in the coordinate system. When the beam center shifts far away from the z-axis and/or the beam profile deviates much from the CGB, more CPU time is required for finishing the BSC computation (typically from 1 h to 10 h on a personal computer). However, the LA method takes about 10 s only.

The capacity of the quadrature method to evaluate the BSCs and to reconstruct the beam field is very sensitive to the orientation of the major axis of elliptical beam cross section (i.e. the angle between the radial vector and the major axis), the beam profile (i.e. the eccentricity of the beam cross section), and the location of the beam center in the coordinate system (i.e. the separation between the beam center and the z-axis). Numerical difficulty appears in the \tilde{I}_m^ϕ calculation because the factor \tilde{I}_m^ϕ is a sum of the modified Bessel functions, in which significant digits may be seriously lost due to the destructive interference of the terms. This takes place when the major axis of the beam cross section is nearly perpendicular to the radial vector \mathbf{r}_0 and the EGB is distant from the z-axis. Therefore, the quadrature method can evaluate the BSCs of the EGB accurately only when the beam center is not too far away from the z-axis or the beam profile does not deviate much from the CGB. The capacity of the LA method is even poorer than the quadrature method, owing to the same reason. Regarding this, we recommend checking the BSC results by comparing the reconstructed beam field with the given one, before the BSCs are used for further calculations of light scattering.

In summary, the formulations of BSCs of an EGB are obtained in terms of 1-dimensional integration of the quadrature method. This method can speed up the numerical computation greatly and acquire reliable results of BSCs as long as the beam center is not too far away from the z-axis and/or the eccentricity of the EGB is not too big.

Acknowledgment

The authors acknowledge the support of the National Natural Science Foundation of China (NSFC51476104). Gratitude is expressed to Shen Li for her helpful suggestions to revise the paper.

Supplementary materials

Supplementary material associated with this article can be found, in the online version, at [doi:10.1016/j.jqsrt.2018.03.026](https://doi.org/10.1016/j.jqsrt.2018.03.026).

References

- [1] Zeng W, Xu M, Zhang Y, Wang Z. Laser sheet drop sizing of evaporating sprays using simultaneous LIEF/MIE techniques. *Proc Combust Inst* 2013;34(1):1677–85.
- [2] Naqwi AA, Liu X, Durst F. Evaluation of the dual-cylindrical wave laser technique for sizing of liquid droplets. *Part Part Syst Charact* 1992;9:44–51.
- [3] Garces-Chavez V, McGloin D, Melville H, Sibbett W, Dholakia K, et al. Simultaneous micromanipulation in multiple planes using a self-reconstructing light beam. *Nature* 2002;419:145–7.
- [4] Grier D. A revolution in optical manipulation. *Nature* 2003;424:810–16.
- [5] Ilić J, Čantrak DJ, Srećković M. Laser sheet scattering and the cameras' positions in particle image velocimetry. *Acta Phys Pol A* 2007;112(5):1113–18.
- [6] Gouesbet G, Gréhan G. Generalized Lorenz-Mie theories. Springer; 2011.
- [7] Gouesbet G, Letellier C, Ren KF, Gréhan G. Discussion of two quadrature methods of evaluating beam-shape coefficients in generalized Lorenz-Mie theory. *Appl Opt* 1996;35:1537–42.
- [8] Gouesbet G, Gréhan G, Maheu B. Expressions to compute the coefficients g_n^m in the generalized Lorenz-Mie theory using finite series. *J Opt* 1988;19:35–48.
- [9] Gouesbet G, Gréhan G, Maheu B. On the generalized Lorenz-Mie theory: first attempt to design a localized approximation to the computation of the coefficients g_n^m . *J Opt* 1989;20:31–43.
- [10] Gouesbet G, Gréhan G, Maheu B. Localized interpretation to compute all the coefficients g_n^m in the generalized Lorenz-Mie theory. *J Opt Soc Am A* 1990;7:998–1007.
- [11] Ren KF, Gouesbet G, Gréhan G. Integral localized approximation in generalized Lorenz-Mie theory. *Appl Opt* 1998;37:4218–25.
- [12] van de Hulst HC. Light scattering by small particles. New York: Wiley; 1957.
- [13] Gouesbet G, Lock JA. Rigorous justification of the localized approximation to the beam-shape coefficients in generalized Lorenz-Mie theory. II. off-axis beams. *J Opt Soc Am A* 1994;11:2516–25.
- [14] Gouesbet G, Lock JA. Comments on localized and integral localized approximations in spherical coordinates. *J Quant Spectr Rad Trans* 2016;179:132–6.
- [15] Ren KF, Gréhan G, Gouesbet G. Evaluation of laser-sheet beam shape coefficients in generalized Lorenz-Mie theory by use of a localized approximation. *J Opt Soc Am A* 1994;11:2072–9.
- [16] Lock JA. Improved Gaussian beam-scattering algorithm. *Appl Opt* 1995;34:559–70.
- [17] Shen J, Jia X. Compact formulation of the beam shape coefficients for elliptical Gaussian beam based on localized approximation. *J Opt Soc Am A* 2016;33(11):2256–63.
- [18] Jia X, Shen J, Yu H. Calculation of generalized Lorenz-Mie theory based on the localized beam models. *J Quant Spectr Rad Trans* 2017;195:44–54.
- [19] Qiu J, Shen J. Beam shape coefficient calculation for a Gaussian beam: localized approximation, quadrature and angular spectrum decomposition methods. *Appl Opt* 2018;57(2):302–13.
- [20] Barton JP, Alexander DR, Schaub SA. Internal and near-surface electromagnetic fields for a spherical particle irradiated by a focussed laser beam. *J Appl Phys* 1988;64:1632–9.
- [21] Ren KF, Gréhan G, Gouesbet G. Electromagnetic field expression of a laser sheet and the order of approximation. *J Opt* 1994;25(4):165–76 Paris.
- [22] Taylor JM, Love GD. Multipole expansion of Bessel and Gaussian beams for Mie scattering calculations. *J Opt Soc Am A* 2009;26(2):278–82.
- [23] Wang JJ, Wriedt T, Maedler L, Han Y, Hartmann P. Multipole expansion of circularly symmetric Bessel beams of arbitrary order for scattering calculations. *Opt Comm* 2017;387:102–9.
- [24] Wen Y, Li Q, Li R, Qin S, Ding C. Scattering of a vector Bessel-Gaussian beam by a sphere. *J Quant Spectr Rad Trans* 2018;204:165–78.
- [25] Ren K-F, Gréhan G, Gouesbet G. Laser sheet scattering by spherical particles. *Part Part Syst Charact* 1993;10:146–51.